

## Multi-Weyl Topological Semimetals Stabilized by Point Group Symmetry

Chen Fang,<sup>1</sup> Matthew J. Gilbert,<sup>2,3</sup> Xi Dai,<sup>4</sup> and B. Andrei Bernevig<sup>1</sup>

<sup>1</sup>*Department of Physics, Princeton University, Princeton, New Jersey 08544, USA*

<sup>2</sup>*Department of Electrical and Computer Engineering, University of Illinois, Urbana, Illinois 61801, USA*

<sup>3</sup>*Micro and Nanotechnology Laboratory, University of Illinois, 208 North Wright Street, Urbana, Illinois 61801, USA*

<sup>4</sup>*Institute of Physics, Chinese Academy of Sciences, Beijing 100080, China*

(Received 30 November 2011; published 27 June 2012)

We perform a complete classification of two-band  $\mathbf{k} \cdot \mathbf{p}$  theories at band crossing points in 3D semimetals with  $n$ -fold rotation symmetry and broken time-reversal symmetry. Using this classification, we show the existence of new 3D topological semimetals characterized by  $C_{4,6}$ -protected double-Weyl nodes with quadratic in-plane (along  $k_{x,y}$ ) dispersion or  $C_6$ -protected triple-Weyl nodes with cubic in-plane dispersion. We apply this theory to the 3D ferromagnet  $\text{HgCr}_2\text{Se}_4$  and confirm it is a double-Weyl metal protected by  $C_4$  symmetry. Furthermore, if the direction of the ferromagnetism is shifted away from the [001] axis to the [111] axis, the double-Weyl node splits into four single Weyl nodes, as dictated by the point group  $S_6$  of that phase. Finally, we discuss experimentally relevant effects including the splitting of multi-Weyl nodes by applying a  $C_n$  breaking strain and the surface Fermi arcs in these new semimetals.

DOI: [10.1103/PhysRevLett.108.266802](https://doi.org/10.1103/PhysRevLett.108.266802)

PACS numbers: 73.20.At

The discovery and classification of topological states of matter beyond those found in time reversal invariant (TRI) materials [1–7] is vital to understanding the full spectrum of possible topological phases. In principle, it is possible to find many more topological systems each containing distinct physical observables characterized by the symmetries they preserve. Nontrivial topology in systems possessing crystallographic point group symmetries (PGS) is of particular interest [8–11] because PGS universally exist in solids, and a classification based on PGS may encompass time-reversal breaking magnetically ordered materials that are useful for potential applications.

Most recently, 3D topological “semimetals” have been proposed to exist in a variety of materials such as cold atom systems [12,13], multilayer topological insulator systems [14,15], and pyrochlore iridates [16,17]. Unlike in a topological insulator, the band structure of a topological semimetal exhibits bulk gapless points in the Brillouin zone (BZ). In close proximity of the gapless points, the effective Hamiltonian is that of a 3D Weyl fermion; therefore, these bulk gapless points are referred to as Weyl nodes [17]. In 3D translationally invariant systems, Weyl nodes are protected from opening a gap against infinitesimal transformations of the Hamiltonian; these points act as monopoles (vortices) of 3D Berry curvature, as any closed 2D surface surrounding them exhibits a unit Chern number, and they can be gapped only by annihilation with other Weyl points of opposite monopole charge. They may exist both in the presence of TRI, as in the metallic state between a TRI trivial and a nontrivial insulator, and in its absence (pyrochlore iridates). Without the presence of any other symmetries, Weyl nodes are the generic topological band crossings in 3D semimetals.

In this Letter, we show theoretically that a series of new 3D topological semimetals may exist when PGS are present

in a material. Physically, this is because PGS can bring together two or multiple Weyl nodes with nonzero net monopole charge together onto a high-symmetry point, resulting in double (quadratic in two directions) or multiple crossings in the BZ. These crossings, which we hereafter denote as “double-Weyl node” or “triple-Weyl node,” are protected from splitting into Weyl nodes by the PGS. We investigate these protected crossings starting from a classification of all two-band  $\mathbf{k} \cdot \mathbf{p}$  theories at high-symmetry points in 3D crystals with a  $C_n$  point group. By applying the classification in 2D, we prove in 2D insulators a relation between the Chern number (mod  $n$ ) and all  $C_m$  eigenvalues of occupied bands at  $C_m$  invariant  $\mathbf{k}$  points in BZ, where  $m$  divides  $n$ . By applying the classification to 3D semimetals, we determine the type of each band-crossing point by knowing the symmetry representations of the conduction and valence bands on high-symmetry lines. As a result,  $C_4$  or  $C_6$  symmetry can protect double-Weyl nodes while only  $C_6$  symmetry can protect triple-Weyl nodes, and there cannot be any higher order crossings protected by  $n$ -fold rotation symmetries. We use this to analyze the recently proposed 3D semimetal  $\text{HgCr}_2\text{Se}_4$  [18] in the ferromagnetic (FM) phase, and find it a  $C_4$ -protected double-Weyl metal with two double-Weyl nodes along  $\Gamma Z$ .

Consider a 3D crystal that is invariant under an  $n$ -fold rotation about the  $z$  axis, where by lattice restriction  $n = 2, 3, 4, 6$ , and containing no other symmetries.  $C_n$  invariance also implies  $C_m$  invariance for any  $m$  divides of  $n$ . In a tight-binding model with translational symmetry,  $C_m$  invariance gives

$$\hat{C}_m \hat{H}(\mathbf{k}) \hat{C}_m^{-1} = \hat{H}(R_m \mathbf{k}), \quad (1)$$

where  $\hat{C}_m$  is the  $m$ -fold rotation operator and  $R_m$  is the  $3 \times 3$  rotation matrix defining the 3D  $m$ -fold rotation. For any  $C_m$ ,

we define a  $C_m$  invariant line on which  $R_m \mathbf{k} = \mathbf{k}$  is satisfied at every  $\mathbf{k}$ . Besides the rotation axis, there exist additional rotation invariant lines due to periodicity of BZ. On any  $C_m$ -invariant line, Eq. (1) implies  $[\hat{C}_m, \hat{H}(\mathbf{k})] = 0$ , such that all bands on the line may be labeled by the corresponding eigenvalues of  $\hat{C}_m$ . If the conduction and valence bands are very close in energy at  $\mathbf{K}$  on a  $C_m$ -invariant line, we can approximate the effective Hamiltonian around that point by a  $2 \times 2$  matrix

$$H_{\text{eff}}(\mathbf{K} + \mathbf{q}) = f(\mathbf{q})\sigma_+ + f^*(\mathbf{q})\sigma_- + g(\mathbf{q})\sigma_z, \quad (2)$$

where  $\mathbf{q}$  is assumed to be small and in plane ( $q_z = 0$ ). The above Hamiltonian is written on the basis where  $(1, 0)^T$  represents the Bloch wave function for the conduction band at  $\mathbf{K}$ , and  $(0, 1)^T$  represents the valence band. In the above equation,  $f$  is a complex function,  $g$  is a real function, and  $\sigma_{\pm} = \sigma_x \pm i\sigma_y$ . On this basis, the matrix representation of  $\hat{C}_m$ ,  $C_m$  is a diagonal matrix with  $(C_m)_{11} = u_c$ ,  $(C_m)_{22} = u_v$ . From Eqs. (1) and (2) and the explicit form of  $C_m$ , we can obtain all symmetry constraints on the functional forms of  $f$  and  $g$ ; however, the full proof is relegated to the Supplemental Material [19]. The constraints and the effective theories to the lowest order of  $\mathbf{q}$  are summarized in Table I. In particular, we note that the constraint on  $g$  always takes the form  $g(q_+, q_-) = g(q_+ e^{i2\pi/m}, q_- e^{-i2\pi/m})$ . This allows a nonzero  $\mathbf{q}$ -independent term,  $g(0) = m(K_z)$ . Therefore, if we know the critical wave vector at which  $m(K_z) = 0$ , then we have a 3D node and the functional forms of  $f$  determine the nature of that node.

Among the various classes of nodes shown in Table I, several cases deserve special attention, as they describe Weyl nodes featuring quadratic and cubic dispersion in  $q_{x,y}$  and carrying  $\pm 2$  and  $\pm 3$  monopole charge, respectively. Consider  $u_c/u_v = -1$  at  $K_z = K_c$  on a  $C_4$ -invariant line, then the effective Hamiltonian, to the lowest order, reads

$$H_{\text{eff}}(\mathbf{q}) = (aq_+^2 + bq_-^2)\sigma_+ + \text{H.c.}, \quad (3)$$

where  $a, b$  are arbitrary complex numbers. Due to the absence of linear terms in Eq. (3), this Hamiltonian describes a double-Weyl node. On a  $C_6$ -invariant line, if  $u_c/u_v = -e^{\pm i2\pi/3}$ , we again have a double-Weyl node at  $K_z = K_c$ . If, however,  $u_c/u_v = -1$ , at  $K_z = K_c$  on a  $C_6$ -invariant line, then the effective Hamiltonian reads

$$H_{\text{eff}}(\mathbf{q}) = (aq_+^3 + bq_-^3)\sigma_+ + \text{H.c.} \quad (4)$$

This describes a triple-Weyl node, as both linear and quadratic terms are absent. We find that no higher order Weyl node beyond triple is protected in 3D. These high-symmetry nodes in a 3D semimetal with  $C_n$  symmetry may be identified by examining the band structure along all  $C_4$ - and  $C_6$ -invariant lines and evaluating  $(u_c, u_v)$  at each crossing point (if any).

Aside from classifying multi-Weyl nodes in 3D semimetals, the results presented in Table I have important implications in 2D Chern insulators. Any  $k_z$  slice ( $k_z \neq k_c$ ) of a 3D system is a 2D insulator with  $k_z$  as a parameter. One may perform a continuous interpolation between different 2D insulators and the interpolation can be mapped onto a 3D BZ using  $k_z$  as the interpolation parameter. Between a 2D Chern insulator and a trivial insulator, the interpolation must have band crossings, which map to nodes in the fictitious 3D BZ. Via Gauss's law, the Chern number of the Chern insulator equals the net monopole charge between the "planes" defining the trivial and Chern insulators. To be more concrete, consider a  $C_4$ -invariant Chern insulator on a square lattice with a band crossing at either  $\Gamma$  or  $M$  with  $C_4$  eigenvalues  $(u_c, u_v)$   $[(u_v, u_c)]$  right before (after) the crossing. If  $u_c/u_v = i$ , then from Table I we obtain a charge of  $+1$ . This means that the Chern number increases by one as the  $C_4$  eigenvalue of the valence band changes by a factor of  $i$ . If  $u_c/u_v = -1$ , then the charge is  $\pm 2$ , and the Chern number changes by  $\pm 2$  as the  $C_4$  eigenvalue changes by a factor of  $-1$ . On the other hand, if the band crossing is at  $C_2$ -invariant point  $X$ , then the charge is always  $\pm 1$ , and, as there are two  $X$ 's in

TABLE I. All two-band  $\mathbf{k} \cdot \mathbf{p}$  theories on  $C_m$ -invariant lines for  $m = 2, 3, 4, 6$  for all possible combinations of  $(u_c, u_v)$ .  $m$  is a real parameter and  $a, b$  are complex parameters that depend on  $K_z$ . Here we provide the general constraints on  $f(q_+, q_-)$  where  $q_{\pm} = q_x \pm iq_y$ . It should be noted that the constraints for  $g$  take a general form:  $g(q_+ e^{i2\pi/m}, q_- e^{-i2\pi/m}) = g(q_+, q_-)$  and are therefore suppressed.

$m$	$u_c/u_v$	Constraints on $f$	$H_{\text{eff}}$	$Q$
2	-1	$f(-q_+, -q_-) = -f(q_+, q_-)$	$m\sigma_z + (aq_+ + bq_-)\sigma_+ + \text{H.c.}$	$\text{sgn}( a  -  b )$
3	$e^{\pm i2\pi/3}$	$f(q_+ e^{i2\pi/3}, q_- e^{i2\pi/3}) = e^{\pm i2\pi/3} f(q_+, q_-)$	$m\sigma_z + ak_{\pm}\sigma_+ + \text{H.c.}$	$\pm 1$
4	$\pm i$	$f(iq_+, -iq_-) = \pm if(q_+, q_-)$	$m\sigma_z + aq_{\pm}\sigma_+ + \text{H.c.}$	$\pm 1$
	-1	$f(iq_+, -iq_-) = -f(q_+, q_-)$	$m\sigma_z + (aq_+^2 + bq_-^2)\sigma_+ + \text{H.c.}$	$2\text{sgn}( a  -  b )$
6	$e^{\pm i\pi/3}$	$f(q_+ e^{i\pi/3}, q_- e^{i\pi/3}) = e^{\pm i\pi/3} f(q_+, q_-)$	$m\sigma_z + aq_+\sigma_+ + \text{H.c.}$	$\pm 1$
	$e^{\pm i2\pi/3}$	$f(q_+ e^{i\pi/3}, q_- e^{i\pi/3}) = e^{\pm i2\pi/3} f(q_+, q_-)$	$m\sigma_z + aq_{\pm}^2\sigma_+ + \text{H.c.}$	$\pm 2$
	-1	$f(q_+ e^{i\pi/3}, q_- e^{i\pi/3}) = -f(q_+, q_-)$	$m\sigma_z + (aq_+^3 + bq_-^3)\sigma_+ + \text{H.c.}$	$3\text{sgn}( a  -  b )$

the BZ, the total Chern number change must be  $\pm 2$ . We may concisely summarize all Chern number changing scenarios for  $C_4$  in one compact formula as

$$\exp(i2\pi C/4) = \prod_{n \in \text{occ}} (-1)^F \xi_n(\Gamma) \xi_n(M) \zeta_n(X), \quad (5)$$

where  $\xi_n$  and  $\zeta_n$  are the  $C_4$  and  $C_2$  eigenvalues on the  $n$ th band, respectively, while  $F = 0$  ( $F = 1$ ) denotes spinless (spinful) fermions. The derivation may be repeated for  $C_{n=2,3,6}$  insulators to obtain

$$\exp(i2\pi C/3) = \prod_{n \in \text{occ}} (-1)^F \theta_n(\Gamma) \theta_n(K) \theta_n(K'), \quad (6)$$

$$\exp(i2\pi C/6) = \prod_{n \in \text{occ}} (-1)^F \eta_n(\Gamma) \theta_n(K) \zeta_n(M), \quad (7)$$

where  $\theta_n$  are the  $C_3$  eigenvalues and  $\eta_n$  are the  $C_6$  eigenvalues on the  $n$ th band. (The definitions of high-symmetry points are as follows:  $\Gamma = (0, 0)$ ,  $X = (\pi, 0)$ ,  $M = (\pi, \pi)$  in  $C_4$  invariant systems,  $K = (0, 4\pi/3\sqrt{3})$ ,  $K' = (0, -4\pi/3\sqrt{3})$ , and  $M = (2\pi/3, 0)$  in  $C_{3,6}$  invariant systems.)

We apply the above general theory to a 3D FM  $\text{HgCr}_2\text{Se}_4$ .  $\text{HgCr}_2\text{Se}_4$  possesses point group  $O_h$  in the paramagnetic phase that breaks down to  $C_{4h}$  in the FM phase. This indicates that the system is invariant under a fourfold rotation about the  $z$  axis, and a mirror reflection about the  $xy$  plane. The band structure calculations show no band crossings along  $XP$ , while along  $\Gamma Z$ , there is a single band crossing at  $k_z = k_c = 0.43a^{-1}$ . In Fig. 1(a), the band structure is plotted with the respective  $C_4$  eigenvalues along  $\Gamma Z$ , and the red point marks the crossing between conduction and valence bands with  $u_c/u_v = -1$ . The crossing point is thus a double-Weyl node with either monopole charge of  $\pm 2$ . This node cannot split into two single Weyl nodes either along the  $z$  axis or in the  $xy$  plane as long as the  $C_4$  symmetry is unbroken. The mirror symmetry about the  $xy$  plane ensures the existence of another double-Weyl node with an opposite monopole charge of  $\mp 2$ . In Fig. 1(b), we plot a schematic of the two double-Weyl nodes in the BZ. The quadratic dispersion along  $k_x$  and  $k_y$  is confirmed by the calculated band dispersion shown in Fig. 1(g). That such double-Weyl node corresponds to a jump of  $\pm 2$  in the Chern number at  $k_z = k_c$  is confirmed in Fig. 1(c), where we calculate the Chern number on a nearest neighbor hopping eight-band tight-binding model on the fcc lattice for  $\text{HgCr}_2\text{Se}_4$  [18].

Additionally, the existence of an  $xy$ -mirror plane implies, for a 3D system, that  $H(k_x, k_y, -k_z) = \mathcal{M}_{xy} H(k_x, k_y, k_z) \mathcal{M}_{xy}^{-1}$ . Hence, at every  $(k_x, k_y)$ , the Hamiltonian  $H(k_x, k_y, k_z)$  possesses 1D inversion symmetry ( $k_z \rightarrow -k_z$ ), which quantizes the electric polarization to be  $P_z(k_x, k_y) = 0$  or  $P_z(k_x, k_y) = 1/2$  depending on the formula  $(-1)^{2P_z} = \prod_{i \in \text{occ}} \zeta_i(0) \zeta_i(\pi)$  [9]. A change of  $P_z$  from 0 to  $1/2$  or vice versa implies crossing a bulk node. In  $\text{HgCr}_2\text{Se}_4$ , we find that at a point very close to

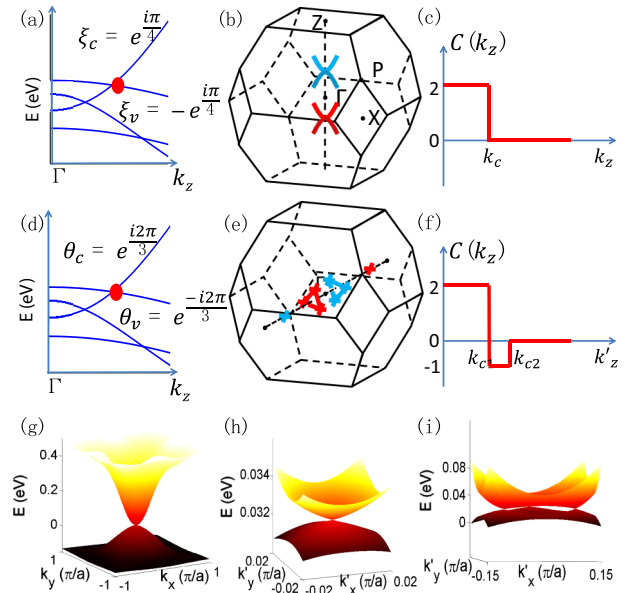


FIG. 1 (color online). (a), (d) Band structure along  $\Gamma Z$  ( $\Gamma L$ ) in 3D FM  $\text{HgCr}_2\text{Se}_4$  with magnetization  $\mathbf{M}$  parallel to  $[001]$  ( $[111]$ ) directions obtained from an eight-band tight-binding model fitted from LDA results. The  $C_4$  ( $C_3$ ) eigenvalues of the conduction and the valence bands are also shown. (b), (e) The schematic showing the two double-Weyl points (four Weyl points) in 3D BZ with  $\mathbf{M}$  parallel to  $[001]$  ( $[111]$ ). Red/darker grey (blue/lighter grey) means nodes with positive (negative) monopole charge(s). (c), (f) The schematic of the Chern number as a function of  $k_z$  ( $k'_z$ ) along  $\Gamma Z$  ( $\Gamma L$ ) with  $\mathbf{M}$  parallel to  $[001]$  ( $[111]$ ). (g) The conduction and the valence band dispersion at  $k_z = k_c = 0.43$  with  $\mathbf{M}$  parallel to  $[001]$ . (h) and (i) The conduction and the valence band dispersion at  $k'_z = k_{c1} = 0.43$  and  $k'_z = k_{c2} = 0.15$  with  $\mathbf{M}$  parallel to  $[111]$ , respectively.

$k_x = k_y = 0$ ,  $P_z(0\pm, 0) = 1/2$  (at  $k_x = k_y = 0$ , the system is gapless at  $k_z = \pm k_c$ ), while at a corner of the BZ,  $P_z(\pi, 0) = 0$ . Therefore, along any path connecting  $(0\pm, 0)$  and  $(\pi, 0)$ , there must be a node. As the path is arbitrary, the result is a line node in the BZ that can only appear on the  $k_z = 0$  or  $k_z = \pi$  plane and is “protected” by  $C_{4h}$  symmetry.

Microscopically, band crossings in  $\text{HgCr}_2\text{Se}_4$  are due to the  $s$ - $p$  orbital inversion in the FM phase [18], but we will show that such inversion alone does not guarantee the existence of double-Weyl nodes. In Fig. 1(d), we plot the band structure along  $\Gamma L$  with ferromagnetism oriented along the  $[111]$  axis [which we now denote as the new  $z'$  direction, in a system  $(x', y', z')$ ]. Figure 1(d) is quite similar to Fig. 1(a); however, the PGS has changed from  $C_{4h}$  to the sixfold rotation-reflection about  $z'$ , or  $S_6 = C_6 * M_{x'y'}$ . This symmetry is different from  $C_6$  and our general theory cannot be directly applied. But noting that  $S_6^2 = C_3$ , we can calculate the  $C_3$  eigenvalues of the conduction and valence bands along  $\Gamma L$  and find  $(u_c, u_v) = (e^{-i2\pi/3}, e^{i2\pi/3})$  [marked in Fig. 1(d)]. This crossing point has a charge  $+1$ , and is, therefore, not a double-Weyl node.

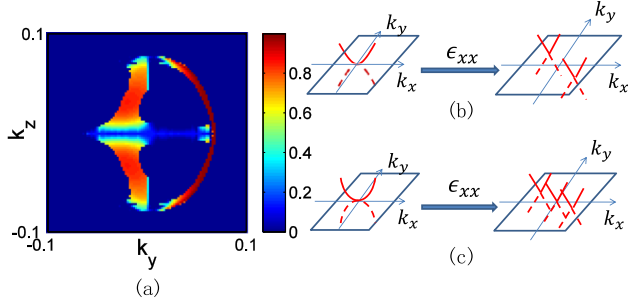


FIG. 2 (color online). (a) Momentum resolved spectral weight,  $\propto \text{Im}[G(k_y, k_z, E)]$ , calculated on the surface of FM  $\text{HgCr}_2\text{Se}_4$  after the system is cut perpendicular to the  $k_x$  direction. The energy is varied as a function of  $k_z$  to ensure that it is inside the bulk gap. The intensity is normalized such that unity means the state is completely localized on the surface. (b) and (c) Schematics showing that a double- and a triple-Weyl node breaks down to two and three Weyl nodes under an applied strain  $\epsilon_{xx}$ , respectively.

Furthermore, on the planes  $k'_z = 0$  and  $k'_z = \sqrt{3}\pi/2a$ , which are invariant under  $M_{x'y'}$  due to the periodicity of BZ,  $C_6$  symmetry is recovered. Using Eq. (7) to evaluate their Chern numbers, we find that  $C(k'_z = 0) = 6n + 2$  and  $C(k'_z = \sqrt{3}\pi/2a) = 6n$ , which implies a net charge of  $-2$  between the two planes. The Weyl node along  $\Gamma L$  at  $k_{c1}$  contributes  $+1$ , so there must be three other Weyl nodes at  $k_{c2}$  related to each other by  $C_3$ , each having a charge  $-1$ . The correct configuration of the bulk nodes is shown in Fig. 1(e). In Figs. 1(h) and 1(i), we plot the linear dispersion around the Weyl point at  $k_{c1}$  and the three Weyl points at  $k_{c2}$ . In going from  $\Gamma$  to  $L$ , the Chern number takes two jumps of  $-3$  and  $+1$  [see Fig. 1(f)]. Physically, the splitting of a double-Weyl node in this case is due to spin-orbital interaction, which is only compatible with  $S_6$  but not  $C_4$  invariance.

In Fig. 2(a) we plot the double-Fermi arcs on the (100)-surface of FM  $\text{HgCr}_2\text{Se}_4$ . Like TRI topological insulators, 3D topological semimetals have surface states. Yet the surface states that cross the Fermi energy do not form a closed loop as in other 2D systems, but appear as Fermi arcs. Specifically, in a Weyl semimetal, if one measures the electron spectral weight on the  $(mnl)$  plane at the Fermi energy, one will see a number of arcs, each of which connects projected images of the two bulk nodes of opposite charge on the  $(mnl)$  plane. When we extend the picture to double- (triple-) Weyl semimetals, there must be two (three) Fermi arcs connecting the two projected images of the two bulk nodes of opposite charge on the  $(mnl)$  plane. The exception to this occurs when the  $[mnl]$  direction is the rotation axis, when the arcs collapse into a single Fermi point.

Another potentially fruitful way to experimentally probe the properties of multi-Weyl semimetals is to examine the quantum phase transitions induced by an applied strain. Since the multi-Weyl nodes studied here are protected by  $C_n$  invariance, an applied strain that breaks such symmetry

can split a multi-Weyl node into several single Weyl nodes. To see how such splitting may happen, consider adding a  $C_4$  breaking term in the effective Hamiltonian around a double-Weyl node, Eq. (3),

$$\Delta H = (\epsilon_{xx} - \epsilon_{yy})\sigma_x. \quad (8)$$

One can check that this term changes sign under  $C_4 \propto \sigma_z$  but is invariant under  $C_2 = C_4^2$ , justifying its coupling to an anisotropic strain  $\epsilon_{xx} - \epsilon_{yy}$ . The dispersion of the adapted Hamiltonian can be easily solved and two nodes emerge at

$$\mathbf{q}_{\pm,c} = (\pm \delta q \cos \theta, \pm \delta q \sin \theta, K_c), \quad (9)$$

where  $\theta$  satisfies  $|a| \sin(\theta_a + 2\theta) = |b| \sin(2\theta - \theta_b)$  and  $\delta q = \sqrt{\epsilon[|a| \cos(\theta_a + 2\theta) + |b| \cos(2\theta - \theta_b)]/2}$ . A straightforward calculation shows that both nodes are Weyl nodes having equal monopole charge  $\text{sgn}(|a| - |b|)$ . In Figs. 2(b) and 2(c), we show, schematically, how a double- (triple-) Weyl node breaks into two (three) Weyl nodes under an anisotropic strain in the  $xy$  plane. This transition is in general marked by the change of density of states  $[\rho(E)]$  near the node, which in principle affects bulk transport properties. For example,  $\rho(E) \propto |E - E_c|$  in double-Weyl semimetals, while  $\rho(E) \propto (E - E_c)^2$  after the splitting by strain, where  $E_c$  is the energy at the node.

C. F. acknowledges travel support by the ONR under Grant No. N0014-11-1-0728 and salary support from ONR under Grant No. N00014-11-1-0635. M. J. G. acknowledges support from the AFOSR under Grant No. FA9550-10-1-0459, the ONR under Grant No. N0014-11-1-0728, and a gift from the Intel Corporation. B. A. B. was supported by NSF CAREER Grant No. DMR-095242, ONR Grant No. N00014-11-1-0635, Darpa Grant No. N66001-11-1-4110, and the David and Lucile Packard Foundation. Xi Dai is supported by NSF China and the 973 Program of China, Grant No. 2011CBA00108. B. A. B. thanks T. L. Hughes and A. Alexandradinata, F. D. M. Haldane, and Z. Fang for fruitful discussions. C. F. thanks W.-F. Tsai and L. Lu for their suggestions for revision.

- 
- [1] C. L. Kane and E. J. Mele, *Phys. Rev. Lett.* **95**, 146802 (2005).
  - [2] C. L. Kane and E. J. Mele, *Phys. Rev. Lett.* **95**, 226801 (2005).
  - [3] B. A. Bernevig, T. L. Hughes, and S. -C. Zhang, *Science* **314**, 1757 (2006).
  - [4] L. Fu, C. L. Kane, and E. J. Mele, *Phys. Rev. Lett.* **98**, 106803 (2007).
  - [5] F. D. M. Haldane, *Phys. Rev. Lett.* **61**, 2015 (1988).
  - [6] J. E. Moore and L. Balents, *Phys. Rev. B* **75**, 121306 (2007).
  - [7] B. A. Bernevig and S. C. Zhang, *Phys. Rev. Lett.* **96**, 106802 (2006).

- [8] A. M. Turner, Y. Zhang, and A. Vishwanath, *Phys. Rev. B* **82**, 241102 (2010).
- [9] T. L. Hughes, E. Prodan, and B. A. Bernevig, *Phys. Rev. B* **83**, 245132 (2011).
- [10] L. Fu, *Phys. Rev. Lett.* **106**, 106802 (2011).
- [11] K. Sun, H. Yao, E. Fradkin, and S. A. Kivelson, *Phys. Rev. Lett.* **103**, 046811 (2009).
- [12] K. Sun, W. V. Liu, A. Hemmerich, and S. D. Sarma, *Nature Phys.* **8**, 67 (2011).
- [13] J. H. Jiang, *Phys. Rev. A* **85**, 033640 (2012).
- [14] G. B. Halasz and L. Balents, *Phys. Rev. B* **85**, 035103 (2012).
- [15] A. A. Burkov and L. Balents, *Phys. Rev. Lett.* **107**, 127205 (2011).
- [16] P. Hosur, S. Ryu, and A. Vishwanath, *Phys. Rev. B* **81**, 045120 (2010).
- [17] X. Wan, A. M. Turner, A. Vishwanath, and S. Y. Savrasov, *Phys. Rev. B* **83**, 205101 (2011).
- [18] G. Xu, H. Weng, Z. Wang, X. Dai, and Z. Fang, *Phys. Rev. Lett.* **107**, 186806 (2011).
- [19] See Supplemental Material at <http://link.aps.org/supplemental/10.1103/PhysRevLett.108.266802> for a detailed proof of results shown in Table I.